



1 **Testing machine learning models for heuristic building damage**
2 **assessment applied to the Italian Database of Observed**
3 **Damage (DaDO)**
4

5 Subash Ghimire¹, Philippe Guéguen¹, Adrien Pothon², Danijel Schorlemmer³

6 ¹ISTerre, Université Grenoble Alpes/CNRS/IRD/Université Gustave Eiffel

7 ²AXA Group Risk Management

8 ³German Research Center for Geosciences, Telegrafenberg, Potsdam, Germany,

9

10 Correspondence to: Subash Ghimire (subash.ghimire@univ-grenoble-alpes.fr)

11

12

13

14

15 **Abstract**

16 Assessing or forecasting seismic damage to buildings is an essential issue for earthquake disaster
17 management. In this study, we explore the efficacy of several machine learning models for damage
18 characterization, trained and tested on the database of damage observed after Italian earthquakes
19 (DaDO). Six regression- and classification-based machine learning models were considered: random
20 forest, gradient boosting and extreme gradient boosting. The structural features considered were divided
21 into two groups: all structural features provided by DaDO or only those considered to be the most
22 reliable and easiest to collect (age, number of storeys, floor area, building height). Macroseismic
23 intensity was also included as an input feature. The seismic damage per building was determined
24 according to the EMS-98 scale observed after seven significant earthquakes occurring in several Italian
25 regions. The results showed that extreme gradient boosting classification is statistically the most
26 efficient method, particularly when considering the basic structural features and grouping the damage
27 according to the traffic-light based system used, for example, during the post-disaster period (green,
28 yellow and red). The results obtained by the machine learning-based heuristic model for damage
29 assessment are of the same order of accuracy as those obtained by the traditional Risk-UE method.
30 Finally, the machine learning analysis found that the importance of structural features with respect to
31 damage was conditioned by the level of damage considered.

32

33 **Key Words**

34 Earthquake building-damage, DaDO building damage database, Machine learning, RISK-UE, Seismic
35 vulnerability of buildings, Italy.



36 1. Introduction

37 Population growth worldwide increases exposure to natural hazards, bringing consequences in terms of
38 global economic and human losses. For example, between 1985 and 2014, the world's population
39 increased by 50% and average annual losses due to natural disasters increased from US\$14 billion to
40 over US\$140 billion. Among other natural hazards, earthquakes represent one-fifth of total annual
41 economic losses and cause more than 20 thousand deaths per year (Daniell et al., 2017; Silva et al.,
42 2019). In order to develop effective seismic risk reduction policies, decision-makers and stakeholders
43 rely on a representation of consequences when earthquakes affect the built environment. Two main risk
44 metrics generally considered at the global scale are associated with building damage: direct economic
45 losses due to costs of repair/replacement and loss of life of inhabitants due to building damage. The
46 necessary damage is estimated by combining the seismic hazard, exposure models and
47 vulnerability/fragility functions (Silva et al., 2019).

48 For scenario-based risk assessment, damage and related consequences are computed for a single
49 earthquake scenario. Many methods to characterize the urban environment for exposure models have
50 been developed. In particular, damage assessment requires vulnerability/fragility functions for all types
51 of existing buildings, defined according to their design characteristics (shape, position, materials,
52 height, etc.) and grouped (for example) in a building taxonomy (e.g. among other conventional methods
53 FEMA, 2003; Grünthal, 1998; Guéguen et al., 2007; Lagomarsino & Giovinazzi, 2006; Mouroux & Le
54 Brun, 2006; Silva et al., 2014). At the regional/country scale, damage assessment is therefore confronted
55 with the difficulty of accurately characterizing exposure according to the required criteria and assigning
56 appropriate vulnerability/fragility functions to building features. Unfortunately, the necessary
57 information is often sparse and incomplete, and exposure modeling is suffering from economic and
58 time constraints.

59 Over the past decade, there has been growing interest in methods using artificial intelligence for seismic
60 risk assessment, due to its superior computational efficiency, easy handling of complex problems, and
61 the incorporation of uncertainties (e.g., Riedel et al., 2014, 2015; Azimi et al., 2020; Ghimire et al.,
62 2022; Hegde and Rokseth, 2020; Kim et al., 2020; Mangalathu & Jeon, 2020; Morfidis & Kostinakis,
63 2018; Salehi & Burgueño, 2018; Sun et al., 2021; Wang et al., 2021; Xie et al., 2020; Y. Xu et al., 2020;
64 Z. Xu et al., 2020). In particular, several studies have tested the effectiveness of machine learning
65 methods in associating damage degrees with basic building features and spatially-distributed seismic
66 demand with acceptable accuracy compared with conventional methods or tested with post-earthquake
67 observations (e.g., Riedel et al., 2014, 2015; Guettiche et al., 2017; Harirchian et al., 2021; Mangalathu
68 et al., 2020; Roeslin et al., 2020; Stojadinović et al., 2021; Ghimire et al., 2022). In parallel, significant
69 efforts have been made to collect post-earthquake building damage observations after damaging
70 earthquakes (Dolce et al., 2019; MINVU, 2021; MTPTC, 2010; NPC, 2015). With more than 10,000
71 samples compiled, the Database of Observed Damage (DaDO), platform of the Civil Protection



72 Department, developed by the Eucentre Foundation (Dolce et al., 2019), allows exploration of the value
73 of heuristic vulnerability functions calibrated on observations (Lagomarsino et al., 2021), as well as the
74 training of heuristic functions using machine learning models (Ghimire et al., 2022) and considering
75 sparse and incomplete building features.

76 The main objective of this study is to investigate the effectiveness of several machine learning models
77 trained and tested on information from the DaDO to develop a heuristic model for damage assessment.
78 The model may be classified as heuristic in the sense that it applies a problem-solving approach in
79 which a calculated guess based on previous experience is considered for damage assessment (as
80 opposed to the application of algorithms which effectively eliminates the approximation). The damage
81 is thus estimated in a non-rigorous way defined during training phase and the results must be validated
82 and then tested against observed damage. By analogy with psychology, this procedure can reduce the
83 cognitive load associated with uncertainties when making decisions based on damage assessment. The
84 dataset and methods are described in the data and method sections, respectively. The fourth section
85 presents the results of damage prediction produced by machine learning models compared with
86 conventional methods, followed by a conclusion section.

87

88 2. Data

89 The Database of Observed Damage (DaDO, Dolce et al., 2019) is accessible through a web-GIS
90 platform and is designed to collect and share information about building features, seismic ground
91 motions and observed damage following major earthquakes in Italy. A framework has been designed
92 to homogenize the different forms of information collected and to translate the damage information into
93 the EMS-98 scale (Grunthal et al., 1998) using the method proposed by Dolce et al. (2019). For this
94 study, we selected building damage data from seven earthquakes summarized in Table 1 and presented
95 in Fig.1.

96

97 **Table 1.** Building-damage data from the DaDO for the seven earthquakes considered in this study. ‘Ref’
98 is the reference of the earthquake used in the manuscript. ‘DL’ is the number of the damage grade
99 available in DaDO. ‘NB’ is the number of buildings considered in this study. AeDES is the post-
100 earthquake damage survey form, first introduced in 1997 and become the official operational tool
101 recognized by the Italian Civil Protection in 2002.

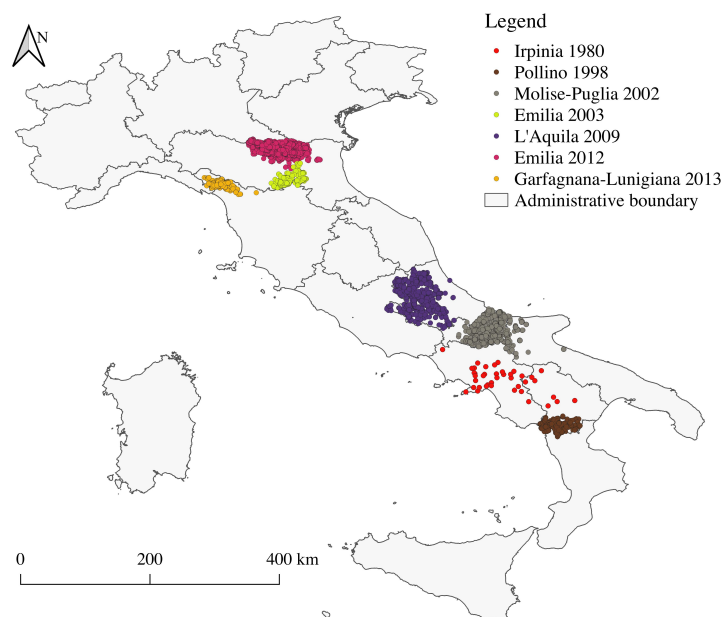
Ref	Earthquake	Event date	Mag.	Epicentre		Damage survey form	DL	NB
				Lat.	Long.			
E1	Irpinia-1980	23/11/1980	6.9	40.91	15.37	Irpinia-980	8	37,828
E2	Pollino-1998	09/09/1998	5.6	40.04	15.98	AeDES-1998	4	9,485
E3	Molise-Puglia-2002	31/10/2002	5.9	41.79	14.87	AeDES-2000	4	6,396
E4	Emilia-Romagna-2003	14/09/2003	5.3	44.33	11.45	AeDES-2000	4	239
E5	L'Aquila-2009	06/04/2009	6.3	42.34	13.34	AeDES-2008	4	37,999
E6	Emilia-Romagna-2012	20/05/2012	6.1	44.89	11.23	AeDES-2008	4	10,581



E7	Garfagnana-Lunigiana-2013	21/06/2013	5.3	44.15	10.14	AeDES-2008	4	1,474
102								
103	The converted damage grade (DG) ranges from damage grade DG0 (no damage) to DG5 (total							
104	collapse). The building features are available for each individual building and relate to the shape and							
105	design of the building and the built-up environment (Tab. 2, Fig. 2), as follows:							
106	Building location - the location of each building is defined by its latitude and longitude, assigned using							
107	either the exact address of the building if available or the address of the local administrative centre							
108	(Dolce et al., 2019).							
109	Numbers of storeys - total numbers of floors above the surface of the ground.							
110	Age of building - time difference between the date of the earthquake and the date of building							
111	construction/renovation.							
112	Height of building - total height of the building above the surface of the ground, in m.							
113	Floor area – average of the storey surface area, in m ² .							
114	Ground slope condition - four types of ground slope conditions are defined (flat, mild slope, steep							
115	slope, and ridge).							
116	Roof type – four types of roofs are defined (thrusting heavy roof, non-thrusting heavy roof, thrusting							
117	light roof, and non-thrusting light roof).							
118	Position of building - indication of the building's position in the block: isolated, extreme, corner, and							
119	intermediate.							
120	Regularity : building regularity in terms of plan and elevation, classified as either irregular or regular.							
121	Construction material : vertical elements: good and poor-quality masonry, good and poor quality							
122	mixed frame masonry, reinforced concrete frame and wall, steel frame, and other.							
123	For features defined as value ranges (e.g., date of construction/renovation, floor area, and building							
124	height), the average value was used. Furthermore, the Irpinia-1980 building damage portfolio (E1) was							
125	constructed using the specific Irpinia-1980 damage survey form, while the AeDES damage survey form							
126	was used for the others. The Irpinia-1980 dataset will therefore be analysed separately.							
127	The data on building damage from earthquake survey other than Irpinia earthquake damage survey							
128	mostly includes damaged buildings. This is because the data was collected based on requests for damage							
129	assessments after the earthquake event (Dolce et al. 2019). The damage information in DaDO database							
130	is still relevant for testing the machine learning models for heuristic damage assessment. Mixing these							
131	datasets to train machine learning models can lead to biased outcomes. Therefore, the machine learning							
132	methods were developed on the other earthquake's dataset excluding Irpinia dataset, and the Irpinia							
133	earthquake dataset was used only in the testing phase.							
134	The distribution of the samples is very imbalanced (Fig. 2): for example, there is a small proportion of							
135	buildings in DG4+DG5 (7.59%), and a large majority of masonry (65.47%) compared to reinforced							
136	concrete frame (21.31%) buildings. This imbalance should be taken into account when defining the							
137	machine learning models.							



138



139

140 **Figure 1.** Geographic location of the buildings considered in this study.

141

142 In order to consider spatially-distributed ground motion, the original DaDO data are supplemented with
 143 the main event macroseismic intensities (MSI) provided by the United States Geological Survey
 144 (USGS) ShakeMap tool (Wald et al., 2005). Macroseismic intensities (MSI) given in terms of modified
 145 Mercalli intensities are considered and assigned to buildings based on their location. The distribution
 146 of MSI values in the database is shown in Fig. 2k.

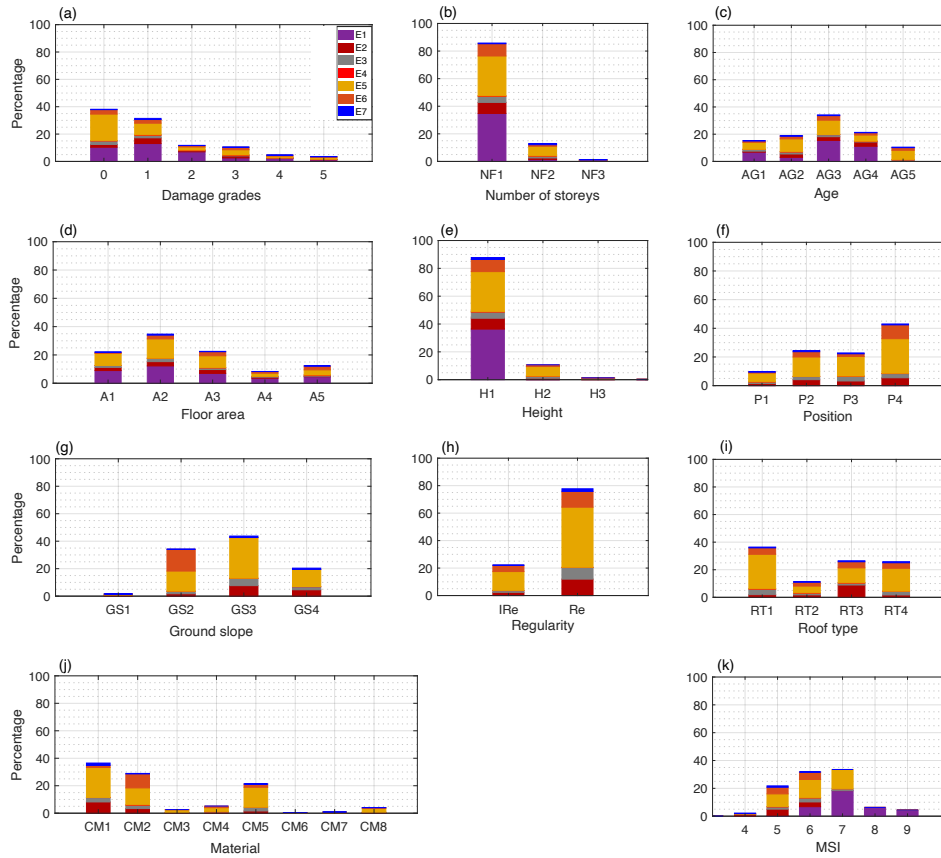
147

148 **Table 2.** Distribution of the different features used in this study.

No.	Parameters	Data type	Distribution (%)	Remarks	
1	No damage	DG0	43.63	Fig. 2a	
	Damage grades (DG)	Slight damage	DG1		28.90
		Moderate damage	DG2		7.41
		Substantial damage	DG3		12.48
		Very heavy damage	DG4		3.94
		Total collapse	DG5		3.65
2	Number of storeys	0-3	NF1	85.81	Fig. 2b
		3-5	NF2	13.01	
		> 5	NF3	1.19	
3	Age (years)	0-20	AG1	15.22	Fig. 2c
		21-40	AG2	18.81	



		41-60	AG3		34.15	
		61-80	AG4		21.34	
		>80	AG5		10.49	
4	Floor area (square metres)	0-50	A1	Numerical	22.16	Fig. 2d
		50-100	A2		34.73	
		100-150	A3		22.53	
		150-200	A4		8.32	
		> 200	A5		12.26	
5	Height (metres)	0-10	H1	Numerical	87.78	Fig. 2e
		10-15	H2		10.69	
		>15	H3		1.50	
6	Position	Corner	P1	Categorical	9.71	Fig. 2f
		Extreme	P2		24.47	
		Internal	P3		22.80	
		Isolated	P4		43.02	
7	Ground slope	Ridge	GS1	Categorical	2.62	Fig. 2g
		Plain	GS2		34.25	
		Moderate slope	GS3		43.74	
		Steep Slope	GS4		20.39	
8	Regularit y	Irregular in plan and elevation	IR	Categorical	22.28	Fig. 2h
		Regular in plan and elevation	Re		77.72	
9	Roof type	Heavy no thrust	R1	Categorical	36.43	Fig. 2i
		Heavy thrust	R2		11.25	
		Light thrust	R3		26.48	
		Light no thrust	R4		25.83	
10	Material	Masonry poor quality	CM1	Categorical	36.51	Fig. 2j
		Masonry good quality	CM2		28.96	
		Mixed frame masonry poor quality	CM3		2.64	
		Mixed frame masonry good quality	CM4		5.21	
		Reinforced concrete frame	CM5		21.31	
		Reinforced concrete wall	CM6		0.42	
		Steel frame	CM7		0.09	
		Other	CM8		4.10	



150

151 **Figure 2.** Distribution of the different features in the database. E1, E2, E3, E4, E5, E6, and E7, representing
 152 Irpinia-1980, Pollino-1998, Molise-Puglia-2002, Emilia-Romagna-2003, L'Aquila-2009, Emilia-Romagna-2012,
 153 and Garfagnana-Lunigiana-2013 building damage portfolios, respectively. The y-axis is the percentage
 154 distribution and the x-axis is (a) Damage grade, (b) Number of storeys (NF1: 0-3, NF2: 3-5, NF3: >5), (c) Building
 155 age (AG1: 0-20, AG2: 21-40, AG3: 41-60, AG4: 61-80, AG5: >80), (d) Floor area (A1: 0-50, A2: 51-100, A3:
 156 101-150, A4: 151-200, A5: >200), (e) Height (H1: 0-10, H2: 10-15, H3: >15), (f) Building position (P1: corner,
 157 P2: extreme, P3: internal, P4: isolated), (g) Ground slope condition (GS1: ridge, GS2: plain, GS3: moderate slope,
 158 GS4: steep slope), (h) Regularity in plan and elevation (IRe: irregular, Re: Regular), (i) Roof type (RT1: heavy
 159 no thrust, RT2: heavy thrust, RT3: light no thrust, RT4: light thrust), (j) Construction material (CM1: poor-quality
 160 masonry, CM2: good-quality masonry, CM3: poor-quality mixed frame masonry, CM4: good-quality mixed
 161 frame masonry, CM5: reinforced concrete frame, CM6: reinforced concrete wall, CM7: steel frames, CM8: other),
 162 and (k) macro-seismic intensity.

163



164 **3. Method**

165 **3.1. Machine learning models**

166 Ghimire et al. (2022) applied classification- and regression-based machine learning models to the
167 damage observed after the 2015 Gorkha Nepal earthquake (NPC, 2015). The main concepts for method
168 selection, definition of the dataset for training and testing, and the representation of model performance
169 are presented here.

170 To develop the heuristic damage assessment model, the damage grades are considered as the target
171 feature. The damage grades are discrete labels, from DG0 to DG5. A label (or class) was thus assigned
172 to the categorical response variables (DG) for the classification-based machine learning models. The
173 three most advanced classification machine learning algorithms were selected: random forest
174 classification (RFC) (Breiman, 2001), gradient boosting classification (GBC) (Friedman, 1999), and
175 extreme gradient boosting classification (XGBC) (Chen and Guestrin, 2016). For the regression-based
176 machine learning models, DG is converted into a continuous variable to minimize misclassifications
177 (Ghimire et al., 2022). The three advanced regression models selected were: random forest regression
178 (RFR) (Brieman, 2001), gradient boosting regression (GBR) (Brieman, 2001), and extreme gradient
179 boosting regression (XGBR) (Chen and Guestrin, 2016).

180 Building features and macroseismic intensities were considered as input features. A one-hot encoding
181 technique was used to convert the categorical features (i.e., ground slope condition, building position,
182 roof type, construction material) into binary values (1 or 0), resulting in 28 input variables (Tab. 2). No
183 input features were removed from the dataset: some building features (e.g., number of storeys and
184 height) may be correlated but we assumed that the presence of correlated features does not impact the
185 overall performance of these machine learning methods (Ghimire et al., 2022). No specific data cleaning
186 methods were applied to the DaDO database.

187 The machine learning algorithms from the Scikit-learn package developed in Python (Pedregosa et al.,
188 2011) were applied. The machine learning models were trained and tested on the randomly selected
189 training (60% of the dataset) and testing (40% of the dataset) subsets of data, considering a single
190 earthquake dataset or the whole DaDO dataset. The testing subset was kept hidden from the model
191 during the training phase.

192

193 **3.2. Machine learning model efficacy**

194 The efficacy of the heuristic damage assessment model (i.e., its ability to predict damage to a
195 satisfactory or expected degree) was analysed in three stages: comparison of the efficacy of the machine
196 learning models using metrics; analysis of specific issues related to machine learning using the selected
197 models; and application of the heuristic model to the whole DaDO dataset.

198

199 **3.2.1 First stage: model selection**



200 In the first stage, only the L'Aquila-2009 portfolio was considered for the training and testing phases.
201 This is the largest dataset in terms of number of buildings and was obtained using the AeDES survey
202 format (Baggio et al., 2007; Dolce et al., 2019). Model efficacy was provided by the confusion matrix,
203 which represents model prediction compared with the so-called "ground truth" value. Accuracy was
204 then represented on the confusion matrix by the ratio of the number of correctly predicted DGs to the
205 total number of observed values per DG (A_{DG}).
206 Total accuracy (A_T) was computed in a similar manner as the ratio of the number of correctly predicted
207 DGs to the total number of observed values. A_T and A_{DG} values close to 1 indicate high efficacy.
208 Moreover, the quantitative statistical error was also calculated as the average of the absolute value of
209 errors (MAE) and the average squared error (MSE) (MAE and MSE values close to 0 indicate high
210 efficacy). For classification-based machine learning models, the ordinal value of the DG was used to
211 calculate the MAE and MSE scores directly. For the regression-based machine learning models, the
212 output DG values were rounded to the nearest integer for the accuracy scores plotted for the confusion
213 matrix, but not for the MAE and MSE value calculations.

214

215 3.2.2 Second stage: machine learning related issues

216 In the second stage, the best heuristic model for damage assessment was selected based on the highest
217 efficacy, and used to analyse and test specific issues related to machine learning: (1) the imbalance
218 distribution of DGs in the DaDO, (2) the performance of the selected model when only some basic, but
219 accurately assessed, building features are considered (i.e., number of storeys, location, age, floor area),
220 and (3) the simplification of the heuristic model, in the sense that DGs are grouped into a traffic-light
221 based classification (i.e., green, yellow and red, corresponding to DG0+DG1, DG2+DG3 and
222 DG4+DG5, respectively). In the second stage, the issues related to machine learning were first analysed
223 using the L'Aquila-2009 portfolio. The whole DaDO dataset was then used.

224

225 3.2.2 Third stage: application to the whole DaDO portfolio and comparison with Risk-UE

226 In the third stage, several learning and testing sequences were considered, with the idea of moving to
227 an operational configuration in which past information is used to predict damage of future earthquakes:
228 either learning based on a portfolio of damage caused by one earthquake and tested on another portfolio,
229 or learning based on a series of damage portfolios and tested on the portfolio of damage caused by an
230 earthquake placed in the chronological continuity of the earthquake sequence considered. In this stage,
231 the efficacy of the heuristic damage assessment model was analysed by comparing the prediction values
232 with the so-called "ground truth" values through the error distribution, as follows:

$$233 \quad \varepsilon_d(\%) = \left(\frac{n_e}{N}\right) * 100 \quad (1)$$

234 where n_e is the total number of buildings at a given error level (difference between observed and
235 predicted DGs), N is the total number of buildings in the damage portfolio.



236 In this stage, the efficacy of the heuristic damage assessment model was compared with the
 237 conventional damage prediction framework proposed by the RISK-UE method (Milutinovic and
 238 Trendafiloski, 2003). The RISK-UE method assigns a vulnerability index (IV) to a building, based on
 239 its construction material and structural properties (e.g., height, building age, position, regularities,
 240 geographic location, etc.). For a given level of seismic demand (MSI), the mean damage (μ_d) and the
 241 probability, p_k , of observing a given damage level k ($k = 0$ to 5) are given by:

$$242 \mu_d = 2.5 \left[1 + \tanh \left(\frac{MSI + 6.25IV - 13.1}{2.3} \right) \right] \quad (2)$$

$$243 p_k = \frac{5!}{k!(5-k)!} \left(\frac{\mu_d}{5} \right)^k \left(1 - \frac{\mu_d}{5} \right)^{5-k} \quad (3)$$

244
 245
 246 Herein, comparing the heuristic model and the RISK-UE method amounts to considering the following
 247 steps, based on the equations given by RISK-UE:

248 **Step 1** - The buildings in the training and testing datasets are grouped into different classes according
 249 to construction material.

250 **Step 2** - For a given building class in the training dataset, computation of

251 **Step 2.1** - mean damage (μ_d) using the observed damage distribution at a given MSI value by:

$$252 \mu_d = \sum_{k=0}^5 p_k k \quad (4)$$

253
 254 **Step 2.2** - vulnerability index (IV) with the μ_d obtained in step 2.1 by:

$$255 IV = \frac{1}{6.25} \left[13.1 - MSI + 2.3 \left(\tanh^{-1} \left(\frac{\mu_d}{2.5} - 1 \right) \right) \right] \quad (5)$$

256
 257 **Step 3** - For the same building class in the test dataset, calculation of

258 **Step 3.1** - mean damage (μ_d) Eq. 2 for a given MSI value with the value of IV obtained in step
 259 2.2;

260 **Step 3.2** - damage probability (p_k) Eq. 3 with the value of μ_d obtained in step 3.1;

261 **Step 3.3** - distribution of buildings in each damage grade within a range of MSI values observed
 262 in the test dataset as follows:

$$263 N_{pred,k} = \sum_{MSI} p_k n_{obs,MSI} \quad (6)$$

264
 265 where $n_{obs,MSI}$ is the total number of buildings observed in the test set for a given MSI
 266 value;

267 **Step 3.4** - absolute error (ϵ_k) in each damage level k , given by:



271
$$\varepsilon_k = \left| \frac{N_{obs,k} - N_{pred,k}}{N} \right| \quad (7)$$

272

273 where, $N_{obs,k}$ is the total number of buildings observed in the given damage grade k .

274

275 Similarly, the heuristic damage assessment model was also compared with the mean damage
 276 relationship (Eq. 4) applied to the test set. Thus, for each building class in the test set, the error value
 277 (Eq. 7) for each DG was computed from the μ_d on the observed damage using Eq. (4), the probability
 278 p_k of obtaining a given DG k ($k= 0$ to 5) using Eq. (3), and the distribution of buildings in each DG
 279 $N_{pred,k}$ for a given MSI value using Eq. (6).

280

281 4. Result

282 4.1 First stage: model selection

283 The efficacy of the regression (RFR, GBR, XGBR) and classification (RFC, GBC, XGBC) machine
 284 learning models trained and tested on the randomly selected 60% (training set) and 40% (test set) of the
 285 2009 -L'Aquila earthquake building damage portfolio is summarized in Table 3. The regression-based
 286 machine learning models RFR, GBR and XGBR yielded similar MSE scores (1.22, 1.22 and 1.21) and
 287 accuracy scores ($A_T = 0.49, 0.49$ and 0.50), considering the five DGs of the EMS-98 scale. In the
 288 confusion matrix (Fig. 2a: RFR, Fig. 2b: GBR, and Fig. 2c: XGBR), the accuracy A_{DG} values show that
 289 the efficacy of these models is higher for the lower DGs (around 60% for DG0 and 55% for DG1) and
 290 lower for the higher DGs (6% and 1% of the buildings are correctly classified in DG4 and DG5,
 291 respectively).

292 For the classification-based machine learning models, the XGBC model ($[MSE, A_T] = [1.78, 0.59]$) was
 293 more effective than the RFC ($[MSE, A_T] = [1.86, 0.57]$) and GBC ($[MSE, A_T] = [1.80, 0.58]$) models,
 294 considering the EMS-98 scale. In the confusion matrix (Fig. 2d: RFC, Fig. 2e: GBC, and Fig. 2f:
 295 XGBC), the accuracy A_{DG} values also show higher model efficacy for the lower DGs (85% for DG0
 296 and 40% for DG1) and lower efficacy for the higher DGs (6%, 12% and 16% buildings correctly
 297 classified in DG2, DG4 and DG5, respectively).

298

299 **Table 3.** Summary of optimized input parameters, accuracy A_T and quantitative statistical error values
 300 for the regression-based and classification-based machine learning methods. The parameters are the
 301 hyperparameters chosen for the machine learning models (the other hyperparameters not mentioned
 302 here are the default parameters in the Scikit-learn documentation (Pedregosa et al., 2011)). The best
 303 accuracy and error values are indicated in bold.

Method	Parameters	Accuracy A_T	MSE	MAE
RFR	n_estimators = 1000	0.49	1.22	0.77

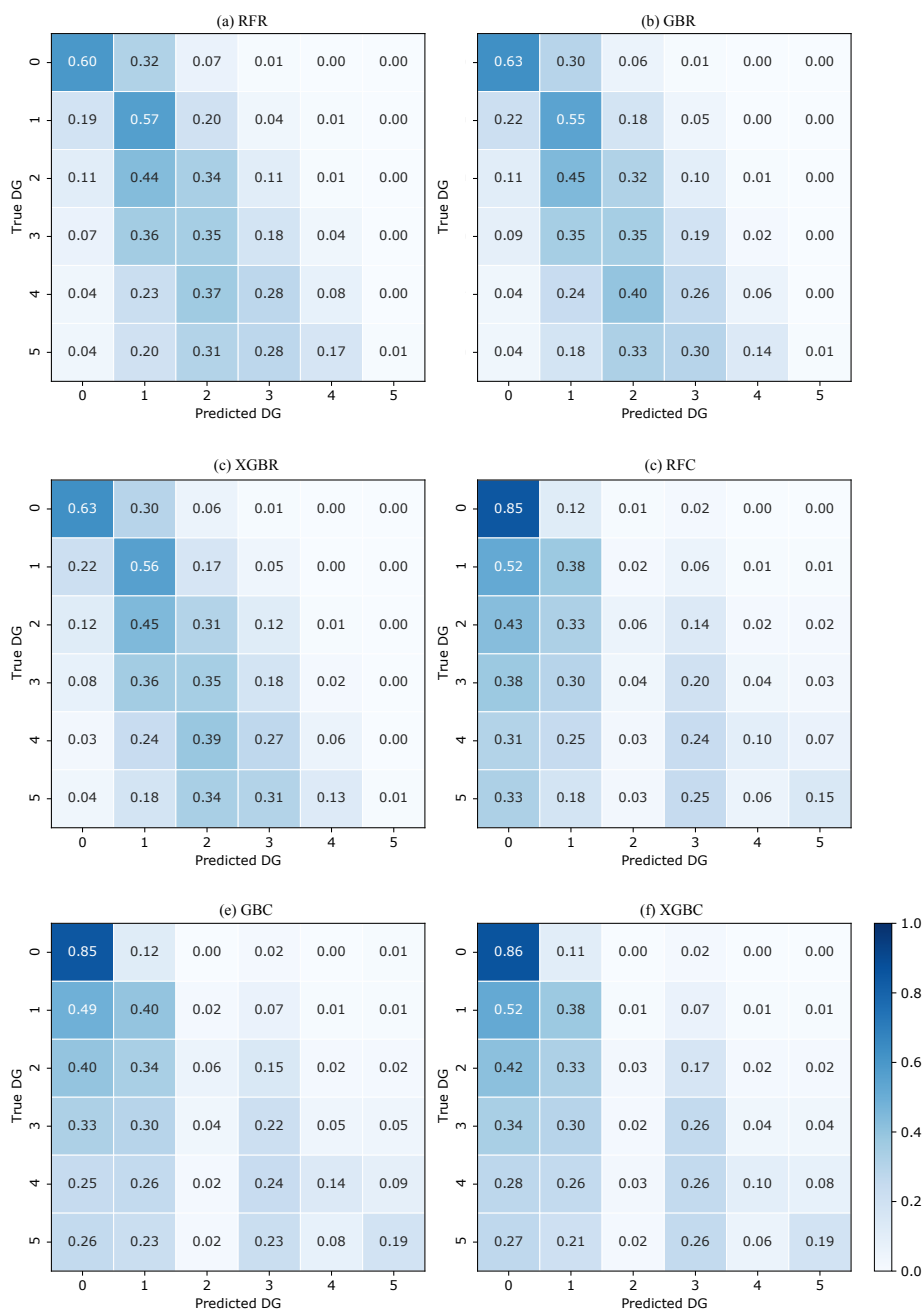


max_depth = 25				
GBR	n_estimators = 1000 max_depth = 10 learning_rate = 0.01	0.50	1.22	0.77
XGBR	n_estimators = 1000 max_depth = 10 learning_rate = 0.01	0.50	1.21	0.76
RFC	no_estimators = 1000 max_depth = 25	0.57	1.86	0.77
GBC	no_estimators = 1000 max_depth = 10 learning_rate = 0.01	0.58	1.80	0.77
XGBC	n_estimators = 1000 max_depth = 10 learning_rate = 0.01	0.59	1.78	0.74

304

305 The classification-based machine learning models thus yielded slightly better predictive efficacy, but
 306 still lower than recent studies applied to other datasets (Ghimire et al., 2022; Harirchian et al., 2021;
 307 Mangalathu et al., 2020; Roeslin et al., 2020; Stojadinović et al., 2021). The high classification error in
 308 the higher DGs could be related to the characteristics of the building portfolio and the imbalance of DG
 309 distribution. Among the classification methods, the XGBC model showed slightly higher classification
 310 efficacy; the XGBC model was therefore selected for the next stages 2 and 3.

311



312

313 **Figure 3.** Normalized confusion matrix between predicted and observed DGs. The values given in each main
 314 diagonal cell are the accuracy scores A_{DG} . All values are also represented by the colour scale.

315

316 **4.2 Second stage: issues related to machine learning**



317 **4.2.1 Imbalance distribution of the DGs in the DaDO**

318 The efficacy of the heuristic damage assessment model depends on the distribution of target features in
 319 the training dataset. This can lead to low prediction efficacy, especially for minority classes (Estabrooks
 320 & Japkowicz 2001; Japkowicz & Stephen 2002; Branco et al. 2017; Ghimire et al., 2022). The previous
 321 section reports significant misclassification associated with the highest DGs for all classification- and
 322 regression-based models (Fig. 3), i.e., for the DGs with the lowest number of buildings (Fig. 2a). The
 323 efficacy of the XGBC model is analysed below, addressing the class-imbalance issue with data
 324 resampling techniques applied to the training phase and considering the L'Aquila-2009 portfolio.

325

326 Four strategies to solve the class imbalance issue were tested:

- 327 (a) random undersampling: randomly selecting the number of data entries in each class equal to the
- 328 number of data entries in the minority class (DG4 in our case);
- 329 (b) random oversampling: randomly replacing the number of data entries in each class equal to the
- 330 number of data entries in the majority class (DG0 in our case);
- 331 (c) Synthetic Minority Oversampling Technique (SMOTE): creating an equal number of data entries in
- 332 each class by generating synthetic samples by interpolating the neighbouring data in the minority class;
- 333 (d) a combination of oversampling and undersampling methods: oversampling of the minority class
- 334 using the SMOTE method, followed by the Edited Nearest Neighbours (ENN) undersampling method
- 335 to eliminate data that is misclassified by its three nearest neighbours (SMOTE-ENN).

336

337 Fig. 4 shows the confusion matrices of the four strategies considered for the class imbalance issue.
 338 Compared with Fig. 3f (i.e., XGBC), the effects of addressing the issue of imbalance were as follows:

- 339 (a) undersampling (Fig. 4a): A_{DG} value increased by 20/22/26% for DG2/DG4/DG5 and decreased by
- 340 29% for DG0.
- 341 (b) oversampling (Fig. 4b): A_{DG} value increased by 11/16/18% for DG2/DG4/DG5 and decreased by
- 342 13% for DG0
- 343 (c) SMOTE (Fig. 4c): A_{DG} value increased by 4/1/4% for DG2/DG4/DG5 and decreased by 3% for
- 344 DG0
- 345 (d) SMOTE-ENN (Fig. 4d): A_{DG} value increased by 13/9/8% for DG2/DG4/DG5 and decreased by 25%
- 346 for DG0.

347 The A_T , MAE and MSE scores are given in Table 4 with the associated effects.

348

349 Table 4 – Scores of the accuracy A_T , MSE and MAE metrics considering the imbalance issue and their
 350 variation Δ compared with values without consideration of the imbalance.

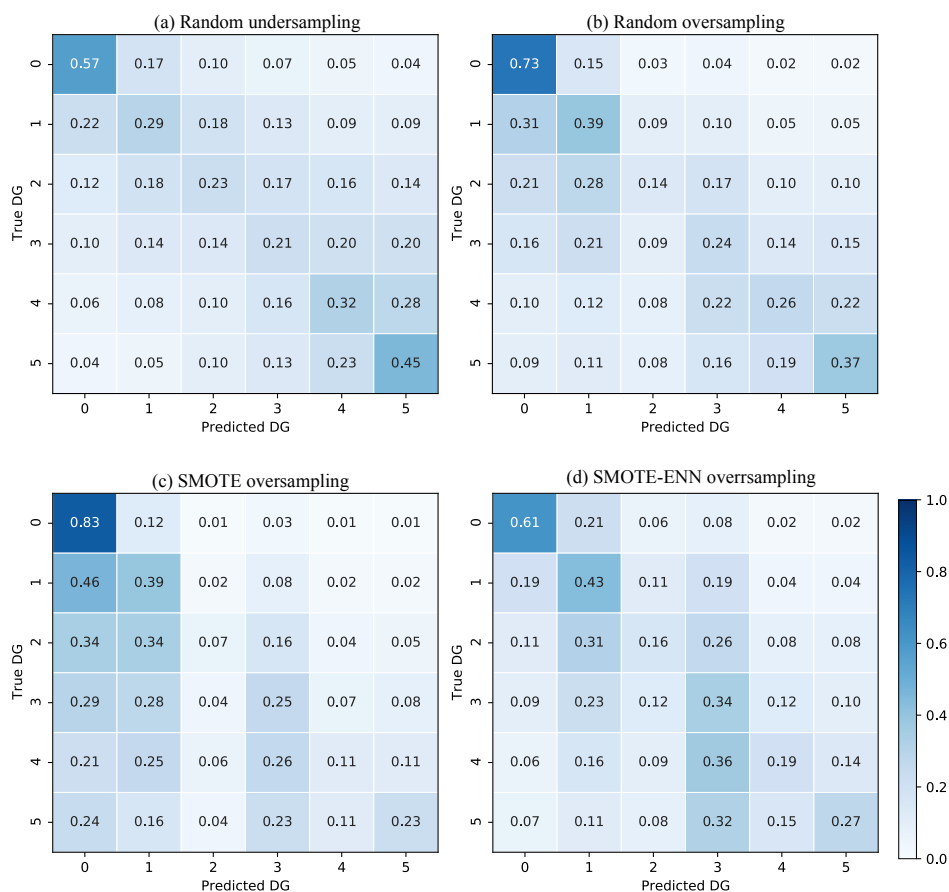
Method	Accuracy A_T		MSE		MAE	
	Scores	Δ	Score	Δ	Score	Δ



Undersampling	0.26	-0.33	1.24	-0.34	1.20	0.46
Oversampling	0.53	-0.06	2.13	0.35	0.86	0.12
SMOTE	0.57	-0.02	1.87	0.09	0.77	0.03
SMOTE-ENN	0.49	-0.10	2.28	0.50	0.93	0.19

351

352 In conclusion, the random oversampling method improves prediction in the minority class without
 353 significantly decreasing prediction in the majority class. The random oversampling method was
 354 therefore applied in this study.



355

356 **Figure 4.** Confusion matrices for the four methods to solve the DG imbalance issue in the DaDO. The values
 357 given in each main diagonal cell are the accuracy scores A_{DG} . All values are also represented by the colour scale.

358

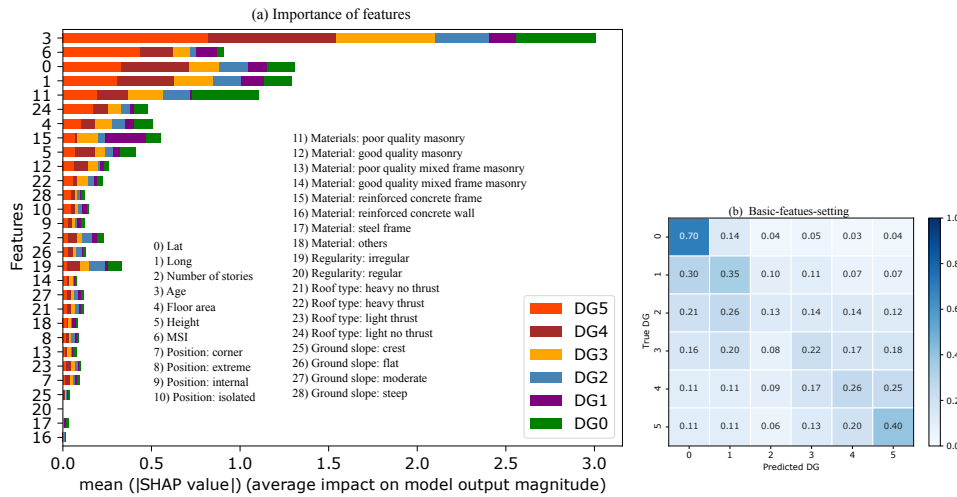
359 **4.2.2 Testing the XGBC model with basic features**



360 This section begins by exploring the importance of each feature in the heuristic damage assessment
361 model applied to the L'Aquila-2009 portfolio. We used the Shapely Additive Explanations (SHAP)
362 method developed by Lundberg and Lee (2017). The SHAP method compares the efficacy of the model
363 with and without considering each input feature to measure its average impact, provided in terms of
364 mean absolute SHAP values.

365 Figure 5a shows the average SHAP value associated with each feature considered in this study as a
366 function of DG. The most weighted features are building age, location (latitude and longitude), material
367 (poor quality masonry, RC frame), MSI, roof type, floor area, and height. Interestingly, the mean SHAP
368 values are dependent on the DG, i.e., the weight of the feature is not linear depending on the DG
369 considered; this is never taken into account in vulnerability methods. For example, Scala et al. (2022)
370 and Del Gaudio et al. (2021) observed a decrease in the vulnerability of structures as construction year
371 increases, without distinguishing the DG considered, which is not the case herein. Note also that the
372 importance score associated with the location feature can capture variations in local geological
373 properties, with buildings serving as low-resolution seismometers for the neighbourhood (Stojadinović
374 et al., 2021), and the vulnerability associated with the built-up area of the L'Aquila-2009 portfolio (e.g.,
375 the distinction between the historic town and more modern urban areas). Furthermore, the average
376 SHAP value obtained for poor quality masonry buildings for DG3/DG4/DG5 confirms the same high
377 vulnerability of this typology as in the EMS-98 scale (Grünthal, 1998), regardless of DG.

378 Some basic features of the building (e.g., location, age, floor area, number of storeys, height) are
379 observed with a high mean SHAP value (Fig. 5a). Compared with others, these five basic features can
380 be easily collected from the field or provided by national census databases, for example. Fig. 5b shows
381 the efficacy of the heuristic damage assessment model using XGBC trained with a set of easily
382 accessible building features (i.e., basic-features-setting: geographic location, floor area, number of
383 stories, height, age, MSI), after addressing the class-imbalance issue using the random oversampling
384 method. Compared with Fig. 4b (considering all features and named the full-features-setting), the
385 XGBC model with the basic-features-setting (Fig. 5b) gives almost the same efficacy with only a 6%
386 average reduction in the accuracy scores.



387

388 **Figure 5.** (a) Graphic representation of the importance scores associated with the different input features
 389 considered for the XGBC model. The features (the same as in Fig. 2) considered in this study are on the y-axis,
 390 and the x-axis is the mean SHAP score according to DG. (b) Confusion matrices considering the basic-features-
 391 setting. The values given in each main diagonal cell are the accuracy scores A_{DG} . All values are also represented
 392 by the colour scale.

393

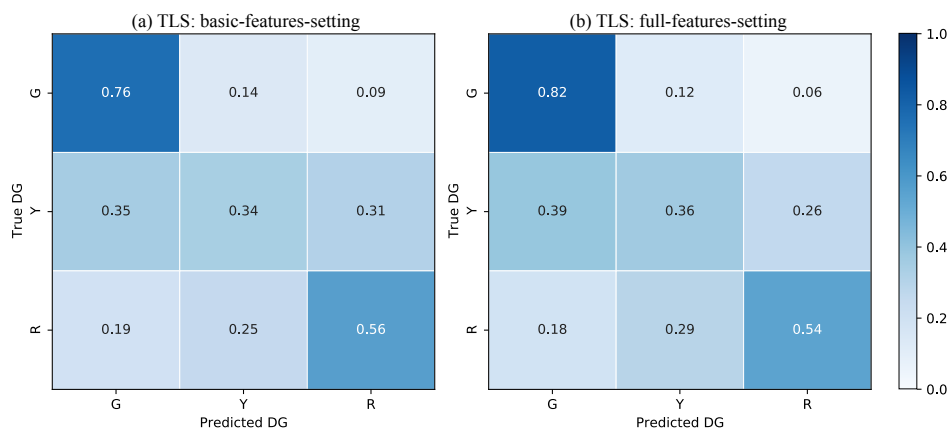
394 4.2.3 Testing the XGBC model with the traffic-light system for damage grades

395 In this section, a simplified version of the DG scale was used, in the sense that the DGs are classified
 396 according to a traffic-light system (TLS) (i.e., green G, yellow Y and red R classes, corresponding to
 397 DG0+DG1, DG2+DG3 and DG4+DG5, respectively), as monitored during post-earthquake emergency
 398 situations (Mangalathu et al., 2020; Riedel et al., 2015; ATC, 2005; Bazzurro et al., 2004). For the
 399 TLS-based damage classification, the XGBC model (after oversampling to compensate of the
 400 imbalance issue) with the basic-features-setting applied to the L'Aquila-2009 portfolio (Fig. 6a) gives
 401 almost the same efficacy compared to the full-features-setting (Fig. 6b). For example, accuracy values
 402 A_{DG} using the basic-features-setting and the full-features-setting were 0.76/0.34/0.56 and 0.82/0.36/0.54
 403 for G/Y/R classes, with the accuracy score A_T of 0.68 and 0.72, respectively. Mangalathu et al. (2020),
 404 Roslin et al., (2020), and Harirchian et al., (2021) reported similar damage grade classification accuracy
 405 values of 0.66, 0.67, and 0.65 respectively.

406 The efficacy of the heuristic damage assessment model using TLS-based damage classification
 407 indicates that classifying damage into three classes is much easier for the machine compared with the
 408 six-class classification system (EMS-98 damage classification). This is also observed during damage
 409 surveys in the field, which sometimes find it hard to distinguish the intermediate damage grades, such
 410 as DG2 and DG3, or DG3 and DG4. Similar observations have been reported in previous studies by



411 Guettiche et al., (2017); Harirchian et al., (2021); Riedel et al., (2015); Roeslin et al., (2020) and
 412 Stojadinović et al., (2021).
 413



414
 415 **Figure 6.** Confusion matrices for (a) the basic-features-setting and (b) the full-features-setting using the traffic-
 416 light (TLS)-based classification, grouping the EMS-98 damage grades (DG) into three classes (green for no or
 417 slight damage; yellow for moderate damage; and red for heavy damage). The values given in each main diagonal
 418 cell are the accuracy scores A_{DG} . All values are also represented by the colour scale.

419

420 4.2.4 Testing the XGBC model with the whole dataset

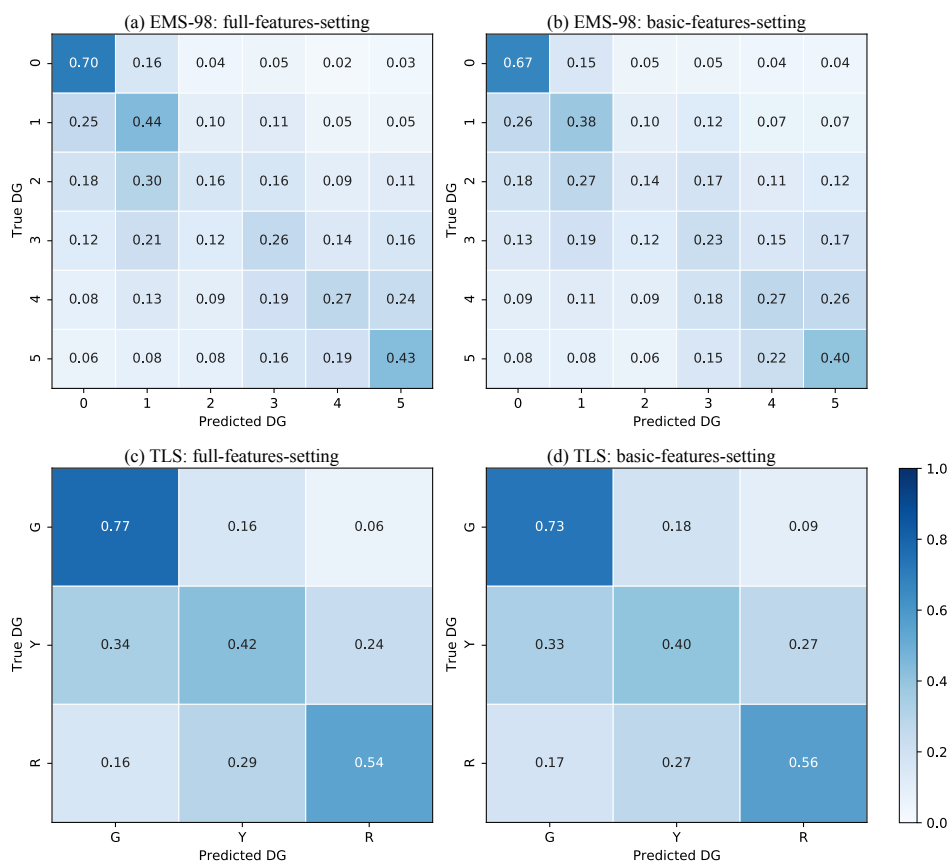
421 The efficacy of the XGBC model was tested using a dataset with six building damage portfolios,
 422 excluding the 1980-Irpinia building damage portfolio. The XGBC model was trained and tested on the
 423 randomly selected 60% (training set) and 40% (test set) of the dataset for EMS-98/TLS damage
 424 classification, with two sets of features (full-features-setting and basic-features-setting), applying the
 425 random oversampling method to compensate for class-imbalance issues. Fig.7 shows the associated
 426 confusion matrix.

427 The basic-features-setting resulted in a similar level of damage prediction compared with the full-
 428 features setting for both EMS-98 and TLS-based damage classification systems. For EMS-98 damage
 429 classification (Fig. 7a, b), the accuracy A_{DG} scores indicated in the confusion matrices are almost the
 430 same for the basic-features-setting and the full-features-setting. Furthermore, the accuracy A_T and MAE
 431 scores are also almost the same (0.45 and 1.08 for the basic-features-setting and 0.48 and 0.95 for the
 432 full-features-setting).

433 Likewise, for TLS-based damage classification (Fig. 7c, d), the accuracy values A_{DG} for the basic-
 434 features-setting and the full-features-setting are almost the same, with similar accuracy A_T and MAE
 435 scores (0.63/0.45 and 0.67/0.39, respectively).

436

437



438

439 **Figure 7.** Confusion matrices for EMS-98 (a, b) and TLS (c, d) damage classification systems using the basic-
 440 and full-features-settings (green for no or slight damage; yellow for moderate damage; red for heavy damage)
 441 with (c) the full-features-setting and (d) the basic-features-setting. The values given in each main diagonal cell
 442 are the accuracy scores A_{DG} . All values are also represented by the colour scale.

443

444 4.3 Third stage: application to the whole DaDO portfolio and comparison with Risk-UE

445 In this section, the efficacy of the heuristic damage assessment model was considered for building
 446 damage predictions, without respecting the time frame of the earthquakes. Two scenarios were
 447 considered: (1) a single building damage portfolio was used for training and the model was then tested
 448 on the others (named single-single), in situations using a single portfolio to predict future damage; and
 449 (2) a number of building damage portfolios were used for training but testing was performed on a single
 450 portfolio (named aggregate-single), i.e. a larger number of damage portfolios were used as a training
 451 set to predict the damage caused by the next earthquake. The model XGBC was applied with the basic-
 452 features-setting (number of storeys, building age, floor area, height, MSI for EMS-98) and EMS-98-
 453 and TLS-based damage classification.



454

455 4.3.1 Single-single scenario

456 First, a series of building damage portfolios, concerning earthquakes occurring in northern or southern
457 Italy and of different magnitudes, was used for training and testing:

458 (i) Training set: E3 – test set: E1, E5, E7.

459 (ii) Training set: E5 – test set: E1, E3, E7.

460 (iii) Training set: E7 – test set: E1, E3, E5.

461

462 Figure 8 shows the distribution of correct DG classification (i.e., $1 - \varepsilon_d$ in % given by Eq. 1) observed
463 for each building for the EMS-98 damage grade (8a) and the TLS (8b) systems. The x-axis represents
464 the incremental error in the damage grade (e.g., 1 corresponds to the delta of damage grade between
465 observation and prediction, regardless of the DG considered).

466 For the EMS-98 damage scale, correct classification (x-value centred on 0) in the range of 31% to 48%
467 was found, depending on the training/test data sets. The error distribution is quite wide with incorrect
468 predictions of +/-1 DG in the range of +/- 13-35%. Remarkably, when considering the E1 portfolio
469 (Irpinia-1980), for which the post-earthquake inventory was based on another form, as the test set, the
470 error is larger. The predictions at +/-1 DG (i.e., the sum of the x-values Fig. 8a between -1 and +1) were
471 70.5%, 69.9% and 72.8% with portfolios E3, E5 and E7 as the test set, respectively, for an average of
472 71%. For the other portfolios, the average of the predictions at +/- 1 DG was 77%, 78% and 77%,
473 respectively, for portfolios E5, E3 and E7 as the test set. This tendency was also observed for the TLS
474 damage system (Fig. 8b). In this case, classification of the E1 portfolio was correct on average (average
475 of x-values centred on 0) at 63% and equal to 72%, 73% and 70.5% for the test on portfolios E5, E3
476 and E7. For both damage scales, the distributions were skewed, with a larger number of predictions
477 being underestimated (positive x-values).

478

479 4.3.2. Aggregate-single scenario

480 Secondly, several aggregated building damage portfolio scenarios were considered to predict a single
481 earthquake, thus testing whether prediction was improved by increasing the number of post-earthquake
482 damage observations. Three scenarios were tested. They are represented in Fig. 9 applying the EMS-98
483 damage grade (9a) and the TLS (9b):

484

485 (i) Training set: E2+E3+E4+E6 (shown as E2346) – test set: E1, E5 and E7.

486 (ii) Training set: E2+E4+E5+E6 (shown as E2456) – test set: E1, E3 and E7.

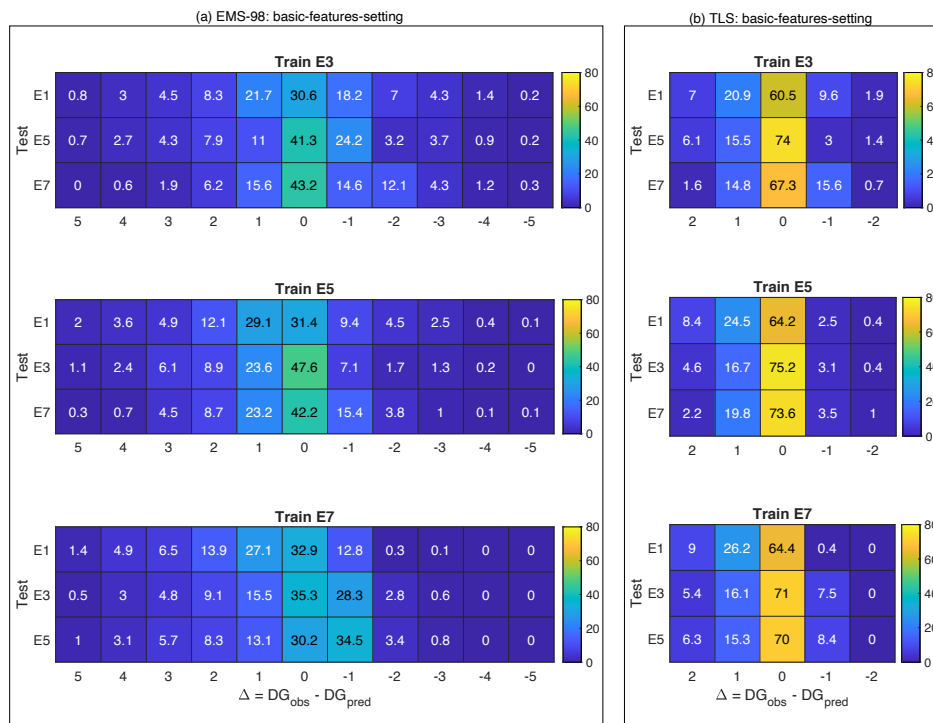
487 (iii) Training set: E2+E4+E6+E7 (shown as E2467) – test set: E1, E3 and E5.

488

489 For the EMS-98 damage scale, correct classification (x-value centred on 0) in the range of 27% to 49%
490 was found, depending on the training/test datasets. As in Fig. 8, using the E1 (Irpinia-1980) earthquake



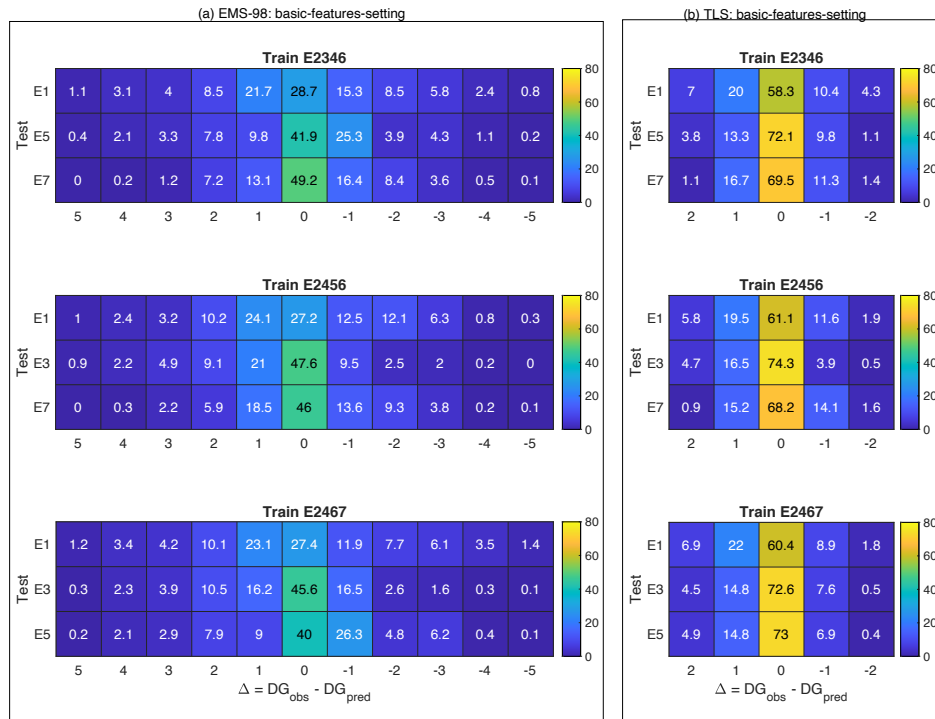
491 for testing scored lower regardless of the portfolio used for training (28.7%, 27.2% and 27.4%
 492 prediction accuracy). With E1 as the test set, the predictions at +/- DG (i.e., the sum of the x-values
 493 on Fig. 9a between -1 and +1) were 65.7%, 63.8% and 62.4% considering the E2346, E2456 and E2467
 494 portfolios as the training set, respectively, for an average of 64% (compared with the 70% score for the
 495 single portfolio scenario, Fig. 8a). Other scenarios were also tested by aggregating the building damage
 496 portfolios differently (not presented herein), leading to the two main conclusions: (1) the quality and
 497 homogeneity of the input data (i.e., building features) affect the efficacy of the heuristic model and (2)
 498 this efficacy is limited and not improved by increasing the number of building damage observations,
 499 with a score (excluding E1) between 40% and 49% (x-value centred on 0), and up to 78% (average of
 500 the two scenarios, Fig. 8a and Fig. 9a) at +/- DG. Considering the TLS damage scale (Fig. 9b), efficacy
 501 of about 72% was obtained (compared with 72% in Fig. 8b), i.e., but no significant improvement was
 502 observed when the number of damaged buildings in the training portfolio was increased. For EMS-98
 503 and TLS, the distributions were skewed, with a larger number of predictions being underestimated
 504 (positive x-values).
 505 Finally, in conclusion, the heuristic damage assessment model based on the XGBC model gives a better
 506 score for TLS damage assessment than for the EMS-98 damage scale. The TLS system also allows for
 507 quick assessment of damage on the large scale such as city or region from an operational point of view.
 508



509



510 **Figure 8.** Distribution of the classification value ($1 - \varepsilon_d$ in % given by Eq. 1) for (a) EMS-98- and (b) TLS-based
 511 damage classification using XGBC machine learning models and considering a single damage portfolio to predict
 512 a single portfolio (single-single scenario). The colour bar indicates the associated value in each cell. The x-values
 513 are the difference between the DG observed and the DG predicted, regardless of the DG considered.
 514



515
 516 **Figure 9.** Distribution of the classification value ($1 - \varepsilon_d$ in % given by Eq. 1) for (a) EMS-98- and (b) TLS-based
 517 damage classification using XGBC machine learning models and considering an aggregate damage portfolio to predict
 518 a single portfolio (aggregate-single scenario). The colour bar indicates the associated value in each cell.
 519 The x-values are the difference between the DG observed and the DG predicted, regardless of the DG considered.

521 4.3.3 Comparing efficacy with the Risk-UE model

522 The efficacy of the heuristic damage assessment model was then compared with conventional damage
 523 prediction methods, i.e., RISK-UE and mean damage relationship (Eq. 2 to 7), considering the basic-
 524 features-settings. For RISK-UE, mean damage μ_d (Eq. 4) was computed using the training set and the
 525 vulnerability index IV for each building (Eq. 5). A vulnerability index was then attributed to all the
 526 buildings in each class defined according to building features. The vulnerability indexes were then
 527 attributed to every building in the test set, mean damage μ_d was computed with Eq. 2 and then DG



528 distribution with Eq. 3, before being compared with the damage portfolio used for testing. Finally, the
529 distribution of the mean damage observed (Eq. 4) was compared with the distribution of damage directly
530 on the test set, using Eq. 3.

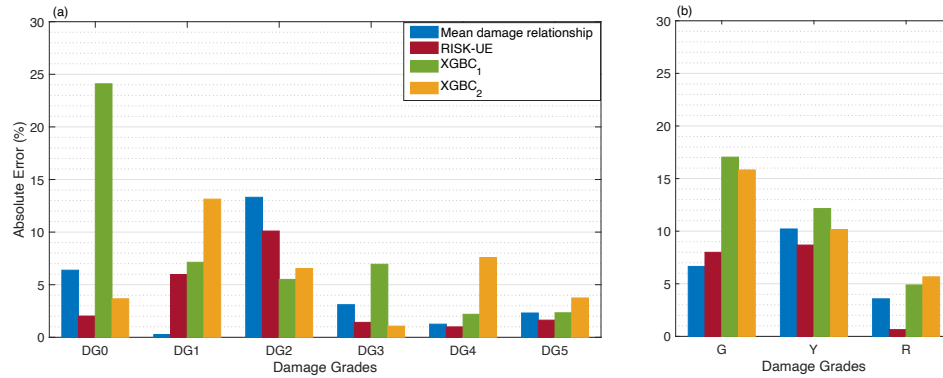
531 Fig. 10 shows the distribution of absolute errors associated with the RISK-UE, mean damage
532 relationship, and XGBC methods (with and without compensation for the class-imbalance issue) trained
533 on earthquake building damage portfolio E5 and tested on E3. For EMS-98 damage classification (Fig.
534 10a), the XGBC model (without compensation for class-imbalance issues) resulted in a level of absolute
535 errors similar to that of the RISK-UE and/or mean damage relationship, except for DG0 (24%). Random
536 oversampling to compensate for the class-imbalance issues improved the distribution of errors for the
537 XGBC model (errors less than 8%, except for DG1: 13%).

538 For TLS-based damage classification, the XGBC model also resulted in a similar level of errors
539 compared with the mean damage relationship and/or RISK-UE methods (Fig. 10b), except for the green
540 class (no or slight damage, 17.04%). Compensation for class-imbalance issues slightly improved the
541 distribution of errors for the XGBC model with a 2% drop in errors for green (no/slight damage) and
542 yellow (moderate damage) classes.

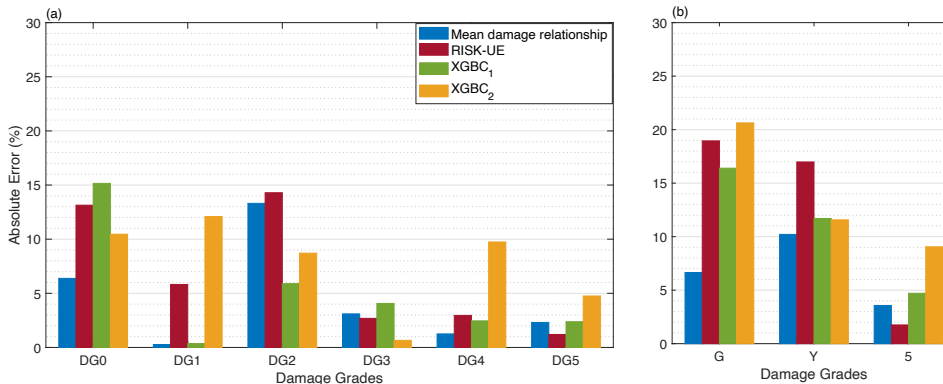
543 Figure 11 shows the distribution of absolute errors trained using the E2456 portfolio and tested on the
544 E3 portfolio. For EMS-98 damage classification (Fig. 11a), the XGBC model (without compensation
545 for class-imbalance issues) resulted in a level of errors similar to that of the RISK-UE and/or mean
546 damage relationship; errors were highest for DG0 with 15.15%. With compensation for the class-
547 imbalance issues, the XGBC model achieved a slightly lower error distribution for DG0 (5%) and DG3
548 (4%); however, for other damage grades, the error value increased significantly (DG1: 11%, DG2: 12%
549 DG4: 7%, DG5: 2%). For TLS-based damage classification, the distribution of absolute errors was
550 similar for both the XGBC model and the mean damage relationship and/or RISK-UE methods (Fig.
551 11b). The highest absolute error value was associated with the green (no or slight damage) class of
552 buildings (16.40%). Compensation for the class-imbalance issues slightly increased the error
553 distribution for the XGBC model with nearly 5% for buildings in the green (no or slight) and red (heavy)
554 classes.

555 These results show that the heuristic building damage model based on the XGBC model, trained using
556 building damage portfolios with the basic-features-setting, provides a reasonable estimation of potential
557 damage, particularly with TLS-based damage classification.

558



559
 560 **Figure 10.** Comparison of the efficacy of the heuristic model with the conventional model considering the DaDO
 561 portfolio (training set: E5; test set: E3) for (a) EMS-98- and (b) TLS-based damage classification. The x-axis is
 562 the damage grade and the y-axis is the percentage of absolute error (ε_k in % given by Eq. 7). The blue bar
 563 corresponds to the mean damage relationship, the red bar corresponds to the RISK-UE method, the green and
 564 orange bars correspond to the heuristic model without (XGBC₁) and with (XGBC₂) compensation for the class-
 565 imbalance issues, respectively.



566
 567 **Figure 11.** Comparison of the efficacy of the heuristic model with the conventional model considering the DaDO
 568 portfolio (training set: E2456; test set: E3) for (a) EMS-98- and (b) TLS-based damage classification. The x-axis is
 569 the damage grade and the y-axis is the percentage of absolute error (ε_k in % given by Eq. 7). The blue bar
 570 corresponds to the mean damage relationship, the red bar corresponds to the RISK-UE method, the green and
 571 orange bars correspond to the heuristic model without (XGBC₁) and with (XGBC₂) compensation for the class-
 572 imbalance issues, respectively.

573

574 5. Conclusion

575 In this study, we explored the efficacy of machine learning models trained using DaDO post-earthquake
 576 building damage portfolios. We compared six machine learning models: RFC, GBC, XGBC, RFR,
 577 GBR, and XGBR. These models were trained on a number of building features (location, number of
 578 storeys, age, floor area, height, position, construction material, regularity, roof type, ground slope



579 condition) and ground motion intensity defined in terms of macro-seismic intensity. The classification
580 models performed slight better than the regression methods and the XGBC model was ultimately found
581 to be optimal. To solve the imbalance issue concerning observed damage, the random oversampling
582 method was applied to the training dataset to improve the efficacy of the heuristic damage assessment
583 model by rectifying the skewed distribution of the target features (DGs).

584 Surprisingly, we found that the weight of the most important building feature evolves according to DG,
585 i.e., the weight of the feature for damage prediction changes depending on the DG considered, which is
586 not taken into account in conventional methods.

587 The basic-features-setting (i.e., considering number of storeys, age, floor area, height and macroseismic
588 intensity, which are accurately evaluated for the existing building portfolio) gave the same accuracy as
589 the full-features-settings with the TLS-based damage classification method. For training and testing,
590 the homogeneity of the information in the portfolios is a key issue for the definition of a highly effective
591 machine, as shown by the data from the E1 earthquake (Irpinia-1990). However, the efficacy of the
592 model reaches a limit which is not improved by increasing the number of damaged buildings in the
593 portfolio used as training set, for example. For damage prediction, this type of heuristic model results
594 in approximately 75% correct classification. Other authors (e.g., Riedel et al., 2014, 2015; Ghimire et
595 al. 2022) have already reached this same conclusion by increasing the percentage of the training set
596 compared with the test set.

597 Despite this limit threshold, the level of accuracy achieved remains similar to that attained by
598 conventional methods, such as Risk-UE and the mean damage relationship, for the basic-features-
599 settings and TLS-based damage classification. Machine learning models trained on post-earthquake
600 building damage portfolios could provide a reasonable estimation of damage for a different region with
601 similar building portfolios.

602 Some variability may have been introduced into the damage prediction model due to the framework
603 defined to translate the original damage scale to the EMS-98 damage scale and because in the DaDO
604 database, the year of construction and the floor area of each building are provided as interval values,
605 and missing locations of buildings were replaced with the location of local administrative centres. The
606 latter can lead to a smoothing of the macro-seismic intensities to be considered for each structure and
607 also affect the distance to the earthquake. Similarly, the building damage surveys were carried out after
608 the seismic sequence, which includes aftershocks as well as the mainshock, whereas the MSI input
609 corresponds to the mainshock from the USGS ShakeMap. All these issues may reduce the efficacy of
610 the heuristic model and its limit threshold. Addressing these issues could improve the damage prediction
611 performance of machine learning models.

612

613 **Code availability**

614 The machine learning models were developed using Scikit-learn documentation and the value of
615 hyperparameters used are provided in table 3.



616 **Data availability**

617 The data used in this study is available in the Database of Observed Damage (DaDO) web-GIS platform
618 of the Civil Protection Department, developed by the Eucentre Foundation.

619 https://egeos.eucentre.it/danno_osservato/web/danno_osservato?lang=EN.

620

621 **Author contribution**

622 Subash Ghimire: Conceptualization, methodology, data preparation, investigation, visualization, draft
623 preparation. Philippe Guéguen: Conceptualization, investigation, visualization, supervision, review and
624 editing. Adrien Pothon: Conceptualization, supervision, review and editing draft. Danijel Schorlemmer:
625 Conceptualization, supervision, review and editing draft.

626

627 **Competing interests**

628 The authors declare that they have no conflict of interest.

629

630 **Acknowledgment**

631 The author(s) disclosed receipt of the following financial support for the research, authorship, and/ or
632 publication of this article: This study was funded by the URBASIS-EU project (H2020-MSCA- ITN-
633 2018, Grant No. 813137). A.P. and P.G. thank the AXA Research Fund supporting the project New
634 Probabilistic Assessment of Seismic Hazard, Losses and Risks in Strong Seismic Prone Regions. P.G.
635 thanks LabEx OSUG@2020 (Investissements d'avenir- ANR10LABX56)

References

636 ATC: ATC-20-1, Field Manual: Postearthquake Safety Evaluation of Buildings Second Edition.,
637 Applied Technology Council, Redwood City, California., 2005.

638 Azimi, M., Eslamlou, A. D., and Pekcan, G.: Data-driven structural health monitoring and damage
639 detection through deep learning: State-of-the-art review, <https://doi.org/10.3390/s20102778>, 2020.

640 Baggio, C., Bernardini, A., Colozza, R., Pinto, A. V, and Taucer, F.: Field Manual for post-earthquake
641 damage and safety assessment and short term countermeasures (AeDES) Translation from Italian:
642 Maria ROTA and Agostino GORETTI, 2007.

643 Bazzurro, P., Cornell, C. A., Menun, C., and Motahari, M.: GUIDELINES FOR SEISMIC
644 ASSESSMENT OF DAMAGED BUILDINGS, in: 13th World Conference on Earthquake Engineering,
645 Vancouver, B.C. m Canada, 74–76, <https://doi.org/10.5459/bnzsee.38.1.41-49>, 2004.

646 Branco, P., Ribeiro, R. P., Torgo, L., Krawczyk, B., and Moniz, N.: SMOGN: a Pre-processing
647 Approach for Imbalanced Regression, *Proc. Mach. Learn. Res.*, 74, 36–50, 2017.

648 Breiman, L.: Random Forests, *Mach. Learn.*, 5–32, 2001.

649 Chen, T. and Guestrin, C.: XGBoost: A Scalable Tree Boosting System, in: 22nd acm sigkdd
650 international conference on knowledge discovery and data mining, 785–794,
651 <https://doi.org/10.1145/2939672.2939785>, 2016.



- 652 Daniell, J. E., Schaefer, A. M., Wenzel, F., and Tsang, H. H.: The global role of earthquake fatalities in
653 decision-making: earthquakes versus other causes of fatalities, Proc. Sixt. world Conf. Earthq. Eng.
654 Santiago, Chile, 9–13, 2017.
- 655 Dolce, M., Speranza, E., Giordano, F., Borzi, B., Bocchi, F., Conte, C., Meo, A. Di, Faravelli, M., and
656 Pascale, V.: Observed damage database of past Italian earthquakes: The da.D.O. WebGIS, Boll. di
657 Geofis. Teor. ed Appl., 60, 141–164, <https://doi.org/10.4430/bgta0254>, 2019.
- 658 Estabrooks, A. and Japkowicz, N.: A mixture-of-experts framework for learning from imbalanced data
659 sets, Lect. Notes Comput. Sci. (including Subser. Lect. Notes Artif. Intell. Lect. Notes Bioinformatics),
660 2189, 34–43, https://doi.org/10.1007/3-540-44816-0_4, 2001.
- 661 FEMA: Hazus –MH 2.1 Multi-hazard Loss Estimation Methodology Earthquake, 2003.
- 662 Friedman, J. H.: Greedy Function Approximation: A Gradient Boosting Machine, 1999.
- 663 Del Gaudio, C., Scala, S. A., Ricci, P., and Verderame, G. M.: Evolution of the seismic vulnerability of
664 masonry buildings based on the damage data from L’Aquila 2009 event, Bull. Earthq. Eng., 19,
665 <https://doi.org/10.1007/s10518-021-01132-x>, 2021.
- 666 Ghimire, S., Gueguen, P., and Schorlemmer, D.: Earthquake Damage Prediction of Buildings in Nepal
667 using Machine Learning Tools, in: VIKAS, A Journal of Development, Nepal’s Post Earthquake
668 Recovery and Reconstruction, special issue, Volume 1, P. 124–131, 2021.
- 669 Ghimire, S., Guéguen, P., Giffard-Roisin, S., and Schorlemmer, D.: Testing machine learning models
670 for seismic damage prediction at a regional scale using building-damage dataset compiled after the 2015
671 Gorkha Nepal earthquake, Earthq. Spectra, <https://doi.org/10.1177/87552930221106495>, 2022.
- 672 Grünthal, G.: Escala Macro Sísmica Europea EMS - 98, 101 pp., 1998.
- 673 Guéguen, P., Michel, C., and Lecorre, L.: A simplified approach for vulnerability assessment in
674 moderate-to-low seismic hazard regions: Application to Grenoble (France), Bull. Earthq. Eng., 5, 467–
675 490, <https://doi.org/10.1007/s10518-007-9036-3>, 2007.
- 676 Guettiche, A., Guéguen, P., and Mimoune, M.: Seismic vulnerability assessment using association rule
677 learning: application to the city of Constantine, Algeria, Nat. Hazards, 86, 1223–1245,
678 <https://doi.org/10.1007/s11069-016-2739-5>, 2017.
- 679 Harirchian, E., Kumari, V., Jadhav, K., Rasulzade, S., Lahmer, T., and Das, R. R.: A synthesized study
680 based on machine learning approaches for rapid classifying earthquake damage grades to rc buildings,
681 Appl. Sci., 11, <https://doi.org/10.3390/app11167540>, 2021.
- 682 Hegde, J. and Rokseth, B.: Applications of machine learning methods for engineering risk assessment
683 – A review, Saf. Sci., 122, 104492, <https://doi.org/10.1016/j.ssci.2019.09.015>, 2020.
- 684 Japkowicz, N. and Stephen, S.: The class imbalance problem A systematic study fulltext.pdf, 6, 429–
685 449, 2002.
- 686 Kim, T., Song, J., and Kwon, O. S.: Pre- and post-earthquake regional loss assessment using deep
687 learning, Earthq. Eng. Struct. Dyn., 49, 657–678, <https://doi.org/10.1002/eqe.3258>, 2020.
- 688 Lagomarsino, S. and Giovinazzi, S.: Macroseismic and mechanical models for the vulnerability and
689 damage assessment of current buildings, Bull. Earthq. Eng., 4, 415–443,
690 <https://doi.org/10.1007/s10518-006-9024-z>, 2006.



- 691 Lagomarsino, S., Cattari, S., and Ottonelli, D.: The heuristic vulnerability model: fragility curves for
692 masonry buildings, Springer Netherlands, 3129–3163 pp., [https://doi.org/10.1007/s10518-021-01063-](https://doi.org/10.1007/s10518-021-01063-7)
693 7, 2021.
- 694 Lundberg, S. M. and Lee, S.-I.: A Unified Approach to Interpreting Model Predictions, in: 31st
695 Conference on Neural Information Processing Systems, 2017.
- 696 Mangalathu, S. and Jeon, J.-S.: Regional Seismic Risk Assessment of Infrastructure Systems through
697 Machine Learning: Active Learning Approach, *J. Struct. Eng.*, 146, 04020269,
698 [https://doi.org/10.1061/\(asce\)st.1943-541x.0002831](https://doi.org/10.1061/(asce)st.1943-541x.0002831), 2020.
- 699 Mangalathu, S., Sun, H., Nweke, C. C., Yi, Z., and Burton, H. V.: Classifying earthquake damage to
700 buildings using machine learning, *Earthq. Spectra*, 36, 183–208,
701 <https://doi.org/10.1177/8755293019878137>, 2020.
- 702 Milutinovic, Z. and Trendafiloski, G.: Risk-UE An advanced approach to earthquake risk scenarios with
703 applications to different european towns, Rep. to WP4 vulnerability Curr. Build., 1–83, 2003.
- 704 Ministry of Housing and Urbanism of Chile, Terremoto y Tsunami 27F 2010:
- 705 Morfidis, K. and Kostinakis, K.: Approaches to the rapid seismic damage prediction of r/c buildings
706 using artificial neural networks, *Eng. Struct.*, 165, 120–141,
707 <https://doi.org/10.1016/j.engstruct.2018.03.028>, 2018.
- 708 Mouroux, P. and Le Brun, B.: Presentation of RISK-UE Project, *Bull. Earthq. Eng.* 2006 44, 4, 323–
709 339, <https://doi.org/10.1007/S10518-006-9020-3>, 2006.
- 710 Ministère des Travaux Publics, Transports et Communications: Evaluation des Bâtiments:
711 https://www.mtptc.gouv.ht/accueil/recherche/article_7.html.
- 712 NPA: Police Countermeasures and Damage Situation associated with 2011Tohoku district - off the
713 Pacific Ocean Earthquake Total burn down Inundated below floor level Partially damaged Property
714 damages Damaged roads Partial burn down March 10, 2021,
715 https://doi.org/https://www.npa.go.jp/news/other/earthquake2011/pdf/higaijokyo_e.pdf (last access: 22
716 March 2021), 2021.
- 717 2015 Nepal Earthquake: Open Data Portal: /eq2015.npc.gov.np/#/, last access: 22 March 2021.
- 718 Pedregosa, F., Varoquaux, G., Buitinck, L., Louppe, G., Grisel, O., and Mueller, A.: Scikit-learn,
719 *GetMobile Mob. Comput. Commun.*, 19, 29–33, <https://doi.org/10.1145/2786984.2786995>, 2011.
- 720 Riedel, I. and Guéguen, P.: Modeling of damage-related earthquake losses in a moderate seismic-prone
721 country and cost–benefit evaluation of retrofit investments: application to France, *Nat. Hazards*, 90,
722 639–662, <https://doi.org/10.1007/s11069-017-3061-6>, 2018.
- 723 Riedel, I., Guéguen, P., Dunand, F., and Cottaz, S.: Macroscale vulnerability assessment of cities using
724 association rule learning, *Seismol. Res. Lett.*, 85, 295–305, <https://doi.org/10.1785/0220130148>, 2014.
- 725 Riedel, I., Guéguen, P., Dalla Mura, M., Pathier, E., Leduc, T., and Chanussot, J.: Seismic vulnerability
726 assessment of urban environments in moderate-to-low seismic hazard regions using association rule
727 learning and support vector machine methods, *Nat. Hazards*, 76, 1111–1141,
728 <https://doi.org/10.1007/s11069-014-1538-0>, 2015.
- 729 Roeslin, S., Ma, Q., Juárez-García, H., Gómez-Bernal, A., Wicker, J., and Wotherspoon, L.: A machine
730 learning damage prediction model for the 2017 Puebla-Morelos, Mexico, earthquake, *Earthq. Spectra*,



- 731 36, 314–339, <https://doi.org/10.1177/8755293020936714>, 2020.
- 732 Salehi, H. and Burgueño, R.: Emerging artificial intelligence methods in structural engineering, *Eng. Struct.*, 171, 170–189, <https://doi.org/10.1016/j.engstruct.2018.05.084>, 2018.
- 734 Scala, S. A., Del Gaudio, C., and Verderame, G. M.: Influence of construction age on seismic vulnerability of masonry buildings damaged after 2009 L’Aquila earthquake, *Soil Dyn. Earthq. Eng.*, 157, 107199, <https://doi.org/10.1016/J.SOILDYN.2022.107199>, 2022.
- 737 Seo, J., Dueñas-Osorio, L., Craig, J. I., and Goodno, B. J.: Metamodel-based regional vulnerability estimate of irregular steel moment-frame structures subjected to earthquake events, *Eng. Struct.*, 45, 585–597, <https://doi.org/10.1016/j.engstruct.2012.07.003>, 2012.
- 740 Silva, V., Crowley, H., Pagani, M., Monelli, D., and Pinho, R.: Development of the OpenQuake engine, the Global Earthquake Model’s open-source software for seismic risk assessment, *Nat. Hazards*, 72, 1409–1427, <https://doi.org/10.1007/s11069-013-0618-x>, 2014.
- 743 Silva, V., Pagani, M., Schneider, J., and Henshaw, P.: Assessing Seismic Hazard and Risk Globally for an Earthquake Resilient World, *Contrib. Pap. to GAR 2019*, 24 p., 2019.
- 745 Stojadinović, Z., Kovačević, M., Marinković, D., and Stojadinović, B.: Rapid earthquake loss assessment based on machine learning and representative sampling, *Earthq. Spectra*, <https://doi.org/10.1177/87552930211042393>, 2021.
- 748 Sun, H., Burton, H. V., and Huang, H.: Machine learning applications for building structural design and performance assessment: State-of-the-art review, *J. Build. Eng.*, 33, 101816, <https://doi.org/10.1016/j.job.2020.101816>, 2021.
- 751 Wald, D. J., Worden, B. C., Quitoriano, V., and Pankow, K. L.: ShakeMap manual: technical manual, user’s guide, and software guide, *Techniques and Methods*, <https://doi.org/10.3133/tm12A1>, 2005.
- 753 Wang, C., Yu, Q., Law, K. H., McKenna, F., Yu, S. X., Taciroglu, E., Zsarnóczy, A., Elhaddad, W., and Cetiner, B.: Machine learning-based regional scale intelligent modeling of building information for natural hazard risk management, *Autom. Constr.*, 122, <https://doi.org/10.1016/j.autcon.2020.103474>, 2021.
- 757 Xie, Y., Ebad Sichani, M., Padgett, J. E., and DesRoches, R.: The promise of implementing machine learning in earthquake engineering: A state-of-the-art review, *Earthq. Spectra*, <https://doi.org/10.1177/8755293020919419>, 2020.
- 760 Xu, Y., Lu, X., Cetiner, B., and Taciroglu, E.: Real-time regional seismic damage assessment framework based on long short-term memory neural network, *Comput. Civ. Infrastruct. Eng.*, 1–18, <https://doi.org/10.1111/mice.12628>, 2020a.
- 763 Xu, Z., Wu, Y., Qi, M. zhu, Zheng, M., Xiong, C., and Lu, X.: Prediction of structural type for city-scale seismic damage simulation based on machine learning, *Appl. Sci.*, 10, <https://doi.org/10.3390/app10051795>, 2020b.
- 766